Experimental Investigation of High Reynolds Number Compressible Axisymmetric Turbulent Wakes

JOEL M. AVIDOR* AND ARTHUR M. SCHNEIDERMAN†
Avco Everett Research Laboratory, Inc., Everett, Mass.

The turbulent axisymmetric wake of a sting has been investigated over a range of Reynolds numbers based on sting length of 7.2×10^6 to 1.54×10^8 and at a freestream Mach number of 2.5. Using a laser Doppler velocimeter (LDV) both mean and RMS velocity fluctuation measurements were carried out up to 160 diameters downstream of the sting base. The streamwise variation of the axis velocity defect defines an extended nonsimilar flow (plateau) region beginning at a Reynolds number of 2×10^7. This region extends to a length of 50 body diameters at the highest Reynolds number studied. The detailed results show the presence of low turbulent intensity and relatively small turbulence macroscale in the plateau region. The present data are consistent with previous wake concentration measurements and are in agreement with theoretical velocity plateau predictions.

Nomenclature

D = sting diameter
f_D = Doppler shifted frequency
L = transverse wake scale
l = plateau length
M = Mach number
r = radial coordinate
$Re_{\infty s}$ = Reynolds number based on sting length
$R(\tau)$ = velocity autocorrelation
u = axial velocity
$\bar{u}$ = mean velocity
u' = turbulence intensity
x = axial coordinate
η = nondimensional radial coordinate (r/L)
θ = scattering angle
λ_o = laser wavelength
Λ = turbulence scale size

Subscripts
∞ = freestream
u = velocity
c = concentration
(o) = on wake axis

Introduction

In recent ballistic range studies of hypersonic, slender cone wakes under conditions of fully turbulent model boundary layers[1] an unusually long nonsimilar (near) wake flow region has been observed. In this region of fully turbulent wake flow, which extended over nearly 100 body diameters, it was found that negligible wake growth and velocity defect decline occurred. (This nonsimilar region is followed by transition to the classical $\frac{1}{3}$ growth similar wake region.) Aside from these ballistic range measurements there appear to be few other observations of an extended wake plateau. Schneiderman[2] has observed a region of negligible growth of the mean concentration of tracer particles in the turbulent wake of a sting. This region extended over a 20 body diameters under conditions of fully turbulent flow along the sting boundary layer.

A purely aerodynamic model has been proposed by Finson.[3] Based upon features of ballistic range shadowgraph data, he postulated that residual boundary-layer turbulence produces an initial wake which is characterized by low-intensity fine-scale turbulence rather than the energetic, large-scale structure which results from the heretofore usual wake transition process. The resulting eddy viscosity is thought to be large enough (small effective Reynolds number) to delay the transition to a self-similar wake by a mechanism involving the damping of large-scale instabilities. Apart from the stability considerations, the eddy viscosity is substantially smaller than the eddy viscosity of self-similar wakes and thereby reduces turbulent diffusion of the wake boundary into the freestream and hence slows the growth of the wake. The nonsimilar plateau, therefore is a region in which the turbulent energy redistributes itself from small to large scales, i.e., it represents a "turbulent" transition between two well established turbulent flows: the boundary layer and the wake.

Much information about axisymmetric wake behavior is now available from experiments carried out in wakes shed by bodies with laminar boundary layers,[4,5] in which case transition to turbulent flow occurs some distance downstream of the base. This information does not apply to the newly observed wake velocity plateau phenomenon which appears to require a turbulent boundary layer on the model. Thus, the present study sought to highlight the effect of boundary-layer turbulence on wake flow characteristics. For this purpose, the compressible turbulent axisymmetric wake of a sting with a fully developed turbulent boundary layer has been investigated; in particular, the presence of a velocity plateau is demonstrated and the detailed flow properties of this region are delineated.

Apparatus, Techniques and Procedures

The experiments described below were carried out in a modified Ludwieg tube[2] which produces 30 ms of flow at a Mach number of 2.5 and a Reynolds number ranging from 3×10^5/in. to 6×10^6/in. based upon 300K stagnation temperature clean air. The model, a $\frac{1}{4}$ in. diam sting, extends 24 in. upstream through the nozzle throat and is supported by streamlined supports in the subsonic portion of the nozzle as shown in Fig. 1. In this way, the effect of the turbulent wakes of the supports is minimized by the inviscid turbulent decay which occurs in the nozzle expansion. In addition the data were obtained in a plane normal to the plane of the supports. Figure 1 also shows the geometry and nomenclature of the experiment.

The measurements were made with a laser Doppler velocimeter (LDV) where the flow velocity at a point was determined by measuring the Doppler shift of monochromatic laser light scattered from small particles introduced into the flow. In the

Received January 9, 1974; revision received October 18, 1974. This research has been supported by U.S. Army, ABMDA, under Contract DAHC60-69-C-0013. We thank T. Cebeci for performing the calculations of the sting boundary-layer flow.

Index categories: Jets, Wakes, and Viscid-Inviscid Flow Interactions; Research Facilities and Instrumentation.

* Principal Research Scientist. Associate Fellow AIAA.
† Principal Research Scientist. Member AIAA.

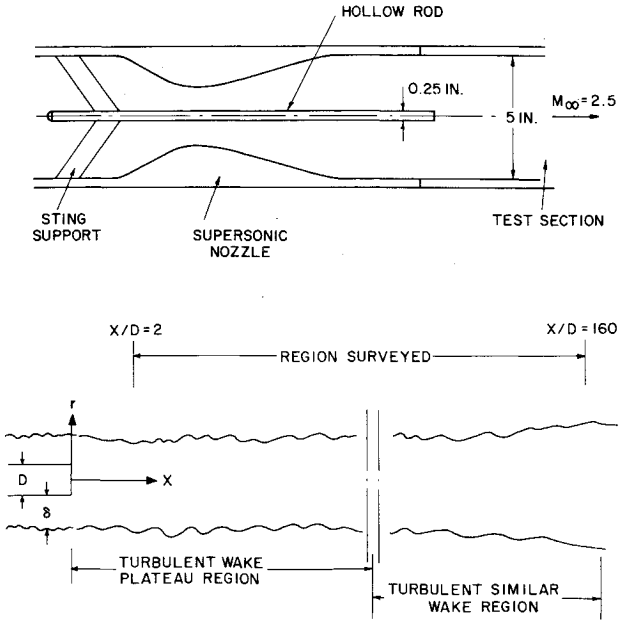

Fig. 1 Experimental arrangement, geometry and nomenclature of the axisymmetric wake experiment.

scattering geometry shown in Fig. 2, the Doppler shift f_D, is given by

$$f_D = (2u/\lambda_o) \sin(\theta/2) \tag{1}$$

where f_D is the Doppler shifted frequency, u the velocity, λ_o the wavelength of the laser, and θ the scattering angle.

Two methods are available for measuring the frequency shift, optical heterodyning and direct spectral analysis using a Fabry-Perot interferometer. In the former, photomultipliers are used as detectors, and because of upper frequency limit ($\sim$100 MHz) of this device, this method becomes difficult to employ in high-speed flow studies where large Doppler shifts in frequency are anticipated. Thus, the second technique was used in the present study.

Two Doppler frequency analyzers based on Fabry-Perot interferometers were incorporated into the present LDV system. For mean and rms velocity measurements a confocal scanning Fabry-Perot interferometer was used. To obtain a continuous time record of the velocity fluctuations needed to generate the higher order turbulence statistics, such as velocity autocorrelation, a novel Doppler frequency analyzer was employed.

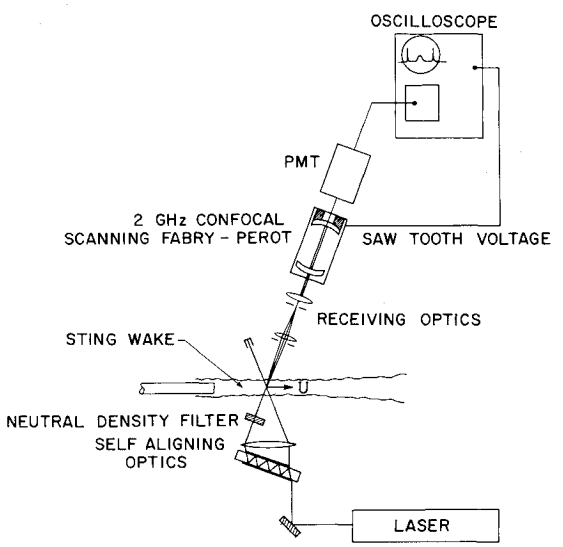

Fig. 2 LDV configuration used in the wake study.

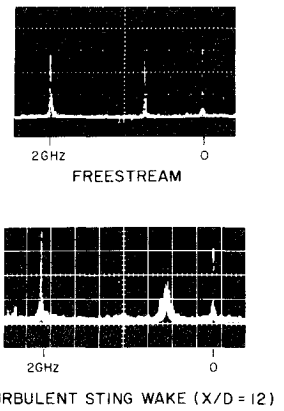

Fig. 3 Typical LDV oscillograms.

The laser Doppler velocimeter developed in the present work is schematically outined in Fig. 2. A single axial mode, argon laser, was used to illuminate the flow borne particles through a self-aligning optical system. This system consists of an optical flat silvered on both sides and a 5 in. diam f1.5 lens, which generates two beams having an intensity ratio of approximately 100:1 and intersecting each other in the test section at a 40° angle at the focal point of the lens. The low intensity beam is used here as the zero velocity marker for the scanning Fabry-Perot as well as for lining up the receiving optics. The receiving optics then transmit the radiation scattered by the flowing particles directly into the velocity detector. These receiving optics consist of an f50 lens, and a 300 μ spatial filter defining an almost spherical probe volume approximately 0.5 mm in diameter.

The scanning spherical Fabry-Perot used here had a 2 GHz free spectral range and a finesse of about 150, yielding a velocity resolution of better than 5 msec. The linear sawtooth voltage from an oscilloscope adjusted to display one order was used to drive the interferometer. The output of which was monitored with a photomultiplier tube (PMT) and recorded on either an oscilloscope or high-speed chart recorder. Figure 3 contains typical data obtained with the scanning Fabry-Perot in the present study. The spike due to the reference beam was used to locate the origin of the velocity axis and the scale was determined using Eq. (1), the known free spectral range, the scattering angle θ, and the laser wavelength λ_o. The abscissa can be shown to be proportional to the probability density function PDF of the velocity fluctuations. The mean velocity is determined from the location of the peak of the PDF while the rms fluctuations are obtained from the half width. In the present study, due to the short test duration (30 ms), the error in the estimate of the rms velocity fluctuations is shown to be about 20% (see Appendix).

The novel Doppler frequency analyzer used here to obtain continuous time records of the velocity fluctuations in the sting wake is described in detail in Ref. 6. It consists of a static slightly defocused spherical Fabry-Perot (DFPS) interferometer used in conjunction with a special mask for the continuous detection of instantaneous Doppler frequency shifts. In this mode of operation introducing the Doppler shifted scattered radiation into the DFPS interferometer results in a fringe pattern of quasi-linearly dispersed rings. The fringe radii are linearly dependent on the Doppler frequency and hence the particle velocity for a system of fixed geometry. Any change in velocity, therefore, will result in a proportional change in the fringe radius, and by monitoring these changes through time, direct velocity fluctuations can be measured. This is achieved here by using a special mask located in front of a photomultiplier on which the fringe pattern is projected. The mask is shaped so that the section of the interference fringe transmitted through it results in a photomultiplier output proportional to the radius. Since at any instant of time the radius is proportional to the Doppler shifted frequency, the photomultiplier output becomes a display of the instantaneous flow velocity. To account for fluctuations in the scattered radiation

Fig. 4 Sting wake laser planograms. $M_\infty = 2.5$, $Re_{\infty s} = 5.4 \times 10^7$, $0 < X/D < 26$.

intensity, the detection system can be modified by introducing a second photomultiplier to sample the total fringe intensity. By dividing the two signals, the fluctuation effect is removed and the divider output becomes the instantaneous velocity display. The divider output is then recorded on a high-speed tape recorder for later data reduction and processing. The frequency response of this Doppler frequency analyzer to velocity fluctuations was found to be better than 500 KHz and that it has a velocity resolution of better than 3 msec.

The particles introduced into the flow to serve as scattering centers were generated using the exploding wire aerosol generator technique described in Ref. 2. Approximately 8000 joules are dumped into an 0.1 gram aluminum strip in a 10 liter chamber containing argon at STP, generating an aerosol which consists of $\sim 0.02\mu$ aluminum particles at a density of about $10^{11}/\text{cm}^3$ in the chamber. It has been shown[2] that this size particles will track flow velocity fluctuation under the given flow conditions well above 1 MHz. The aluminum aerosol is prepared several minutes before use to allow it to reach a uniform state and is premixed into the driver section of the tunnel so that the entire flow, both wake and freestream, contain tracer particles. The mass loading of the flow due to the presence of the aluminum particles was about 10^{-3}.

Results and Discussion

Some near wake planograms of the turbulent sting wake taken at $Re_{\infty s} = 5.4 \times 10^7$ are presented in Fig. 4. The data obtained using the laser planogram technique[7] suggest that the sting wake does not grow in the region of $0 < X/D < 26$, also the qualitative behavior of the wake boundary is substantially less rugged compared to what has been observed further downstream in the sting wake under identical flow conditions.[2]

The axial variation of the wake velocity defect as function of X/D for $Re_{\infty s} = 7 \times 10^6$ and 5.4×10^7 are shown in Fig. 5. The most interesting fact in this figure is that for the high Reynolds number case, the velocity defect data exhibits a "plateau," remaining constant for more than 20 body diameters, and later decays as $(x/D)^{-2/3}$ in agreement with a self-preserving wake. At this Reynolds number the sting boundary layer is fully turbulent so that this "near wake" region cannot be a transition region from a laminar to a turbulent wake. Also the measurements carried out in this region show the flow in the plateau to be fully turbulent, so that relaminarization of the flow cannot account for this observed phenomena either. In the lower Reynolds number case, it is seen that at about 2 sting diameters

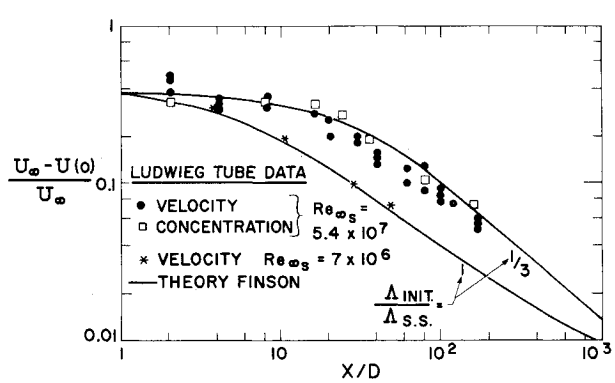

Fig. 5 Axial variation in velocity defect.

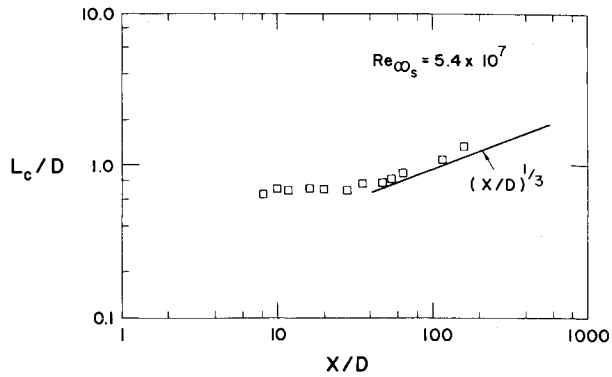

Fig. 6 Axial variation of transverse scale.

downstream of the base the velocity starts to decay and the axial variation also shows an $(x/D)^{-2/3}$ dependence. Using the method employed by Demetriades[5] to determine the virtual wake origin, X_o, in which one extrapolates the axial velocity distribution in Fig. 5 to $[u_\infty - u(o)]/u_\infty = 1$, puts the origin for both cases at about 1 diam downstream of the sting base. Hence differences in virtual wake origin could not account for the difference in near wake behavior between the two cases presented in Fig. 5.

Mean concentration measurements previously carried out in the sting wake using the laser planogram technique[2] are included in Fig. 5. It is seen that the velocity and concentration data agree well with each other as would be expected. However, it should be mentioned here that the concentration data were in a normalized form, thus having an arbitrary level associated with it, so that for the comparison carried out in this work the arbitrary level was selected to overlay the velocity defect measurements.

The axial variation of the transverse wake scale (L_c) obtained from the concentration measurements is shown in Fig. 6. The above data also shows that for the first 20–30 body diameters, the transverse scale remains constant. This region is coincident with the velocity and concentration plateau region. Following this region, the wake growth as a self-similar wake, such that L_c/D increases as $(X/D)^{1/3}$.

As pointed out an estimate of the rms velocity fluctuations can be obtained from the LDV data. The axial variation of the turbulence intensity in the wake is shown in Fig. 7. As is seen from this figure, the flow in the plateau region is turbulent, and the turbulent intensity is approximately constant with a value of about 25% of the velocity defect. By way of comparison, Demetriades, in his sting wake study carried out at $M_\infty = 3$ and under laminar sting boundary-layer flow conditions, measured fluctuating velocities equal to 50% of the velocity defect.

Recently, preliminary turbulence macroscale data for the $Re_{\infty s} = 5.4 \times 10^7$ case only, also have been obtained. Using the novel LDV velocity detector, continuous velocity fluctuation data in the plateau and self-similar wake regions have been recorded. These data were then used to generate longitudinal velocity autocorrelations, from which the turbulence scale size was obtained. Invoking Taylor's hypothesis of frozen convection

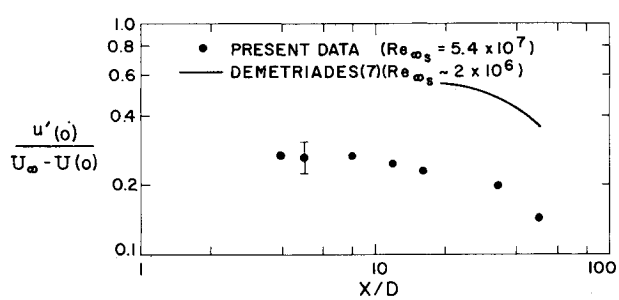

Fig. 7 Axial variation of rms velocity.

the longitudinal integral scale of the velocity was computed from the velocity autocorrelations and the local mean velocity using the following relation:

$$\Lambda = \bar{u} \int_o^\infty R(\tau)\, d\tau \qquad (2)$$

It was found that under these flow conditions the macroscale values on the wake axis in the plateau ($X/D = 12$) and self-similar ($X/D = 80$) wake regions are $\Lambda/D \cong 0.25$ and $\Lambda/D \cong 0.7$, respectively. The present result for the macroscale in the self-similar wake region agree closely with existing data.[4,8] However, in the plateau region the measured turbulence scale size is substantially smaller than has been previously observed.

We may illustrate the observed nature of the near wake turbulence (namely low turbulence intensity and small turbulence scale size), by estimating and accounting for the turbulent sting boundary-layer turbulence shed into the near wake. Based on freestream conditions the turbulence intensity in the plateau is about 10% of the freestream velocity, a result that compares well with recent measurements of velocity fluctuation level in a thick axisymmetric turbulent boundary layer.[9] In this study, Patel et al.[9] have found that a relatively low level of turbulence exists in the thick boundary layer near the tail of an axisymmetric body as compared to a thin boundary layer that is proceeding towards separation where the velocity fluctuations and shear stresses are much larger. Using the numerical solution of Cebeci[10] for thick axisymmetric turbulent boundary-layer flows, the mean flow properties of the sting boundary layer were calculated. The results show that at the sting base the boundary-layer thickness is about the size of the sting diameter. Assuming the turbulence macroscale to be about 20% of δ, as has been observed in flat plate flows[11-13] yields $\Lambda/D \cong 0.2$, a result in qualitative agreement with the present plateau macroscale data. These similarities in turbulent intensity and scale size thus indicate that in the present case ($Re_{\infty s} = 5.4 \times 10^7$) the turbulence in the plateau region is dominated by sting boundary-layer turbulence.

In order to compare our axial velocity defect measurements in the wake, Finson's model[3] for high Reynolds number wake aerodynamics was applied to our geometry. Inputs to this calculation are the fluctuation intensity and turbulent scale size. Using the values measured in the wake plateau, namely; $u'/[u_\infty - u(o)] = 0.25$ and Λ initial/Λ self-similar $= \frac{1}{3}$, numerical results were obtained. The results included in Fig. 5 agree very well with the measured axial velocity defect variation. For the lower Reynolds number case, using the same turbulence intensity as measured at $Re_{\infty s} = 5.4 \times 10^7$ and assuming an initial turbulence macroscale Λ initial/Λ self-similar $= 1$ yields in this case the best fit to the measured data. This suggests that under these flow conditions the dominant turbulence scale size in the near wake region is substantially larger than in the high Reynolds number case where a velocity plateau has been observed.

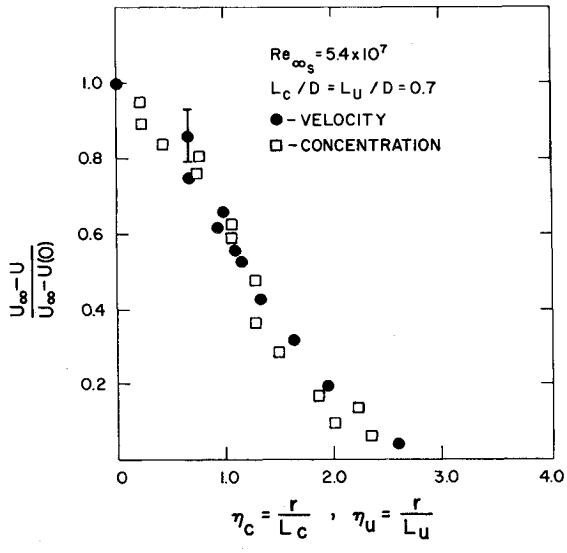

Fig. 8 Radial velocity and concentration distribution in the plateau region ($X/D = 12$).

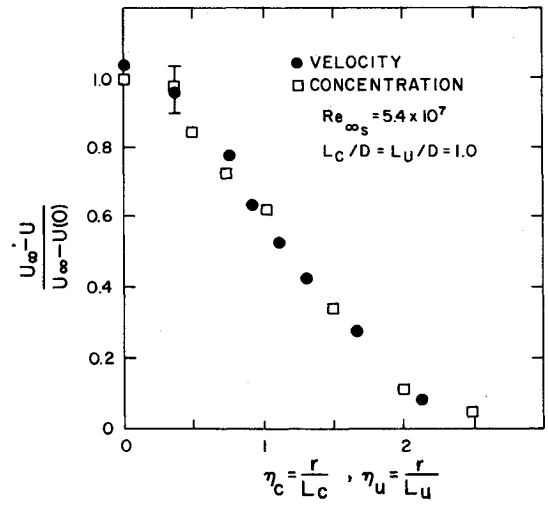

Fig. 9 Radial velocity and concentration distribution in the self-similar region ($X/D = 80$).

The combined radial variation of the velocity and concentration measured in the plateau ($X/D = 12$) and self-similar ($X/D = 80$) wake regions are presented in Figs. 8 and 9. The radial coordinate of each was nondimensionalized using the appropriate transverse wake scale. In both cases, the velocity and concentration profiles are in good agreement with each other, indicating that the velocity transverse scale is equal to the concentration scale, and both are Gaussian in the plateau region of the wake. Similarity is not, however, reached in this region of the flow as the wake velocity and the wake growth data indicate.

An estimate of the radial rms velocity variation in the plateau ($X/D = 12$) is presented in Fig. 10. The turbulent intensity profile is of the same size as the velocity profile indicating that the full velocity profile is turbulent. Also the velocity fluctuations normalized with the axis values show that the maximum value of the fluctuations occur at $\eta \cong 1.0$; the point of maximum

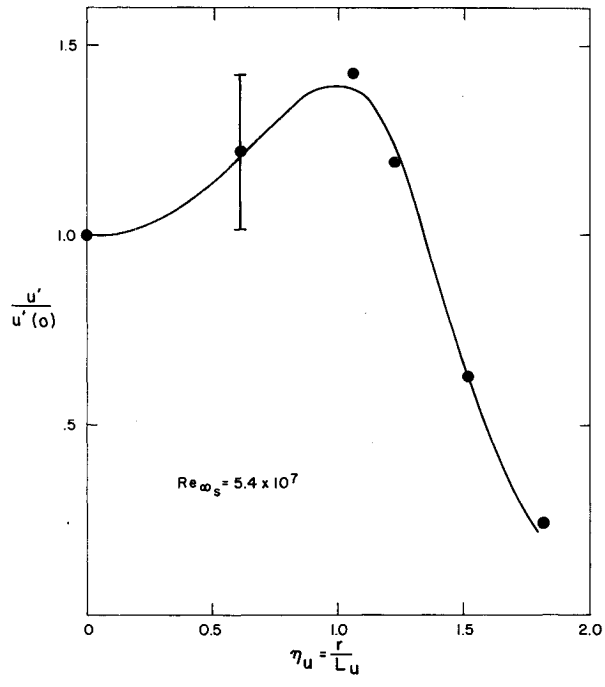

Fig. 10 Radial variation of rms velocity in the plateau region ($X/D = 12$).

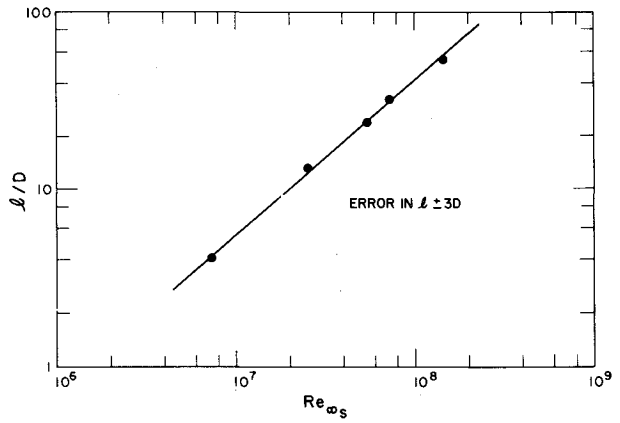

Fig. 11 Plateau length vs sting Reynolds number.

shear, similar to behavior observed in the self-similar wake region.[8]

By varying the Reynolds number of the flow it was found that the plateau length increases and decreases with the respective increase or decrease in Reynolds number, $Re_{\infty s}$. These results are shown in Fig. 11 where the longest plateau observed was $l/D = 50$ at $Re_{\infty s} = 1.54 \times 10^8$. The plateau length for a given Reynolds number was determined by intersecting the $(X/D)^{-2/3}$ slope line of the self-preserving region of the wake with the flat line of the plateau region. From the data, the length of the so-called "plateau" region in this study can be related to the sting Reynolds number $Re_{\infty s}$ in the following manner:

$$l/D \cong 40(Re_{\infty s}/10^8) \tag{3}$$

Conclusions

The following conclusions can be drawn regarding the high Reynolds number wake experiment:

1) An unusually long nonsimilar wake flow region has been observed; in this region of fully turbulent flow, it was found that negligible wake growth and velocity defect decay occurred. Following this so-called plateau region, the wake velocity defect and concentration decay in a manner approaching the inverse $\frac{2}{3}$ decay law characteristic of the axisymmetric similar turbulent wake.

2) Mean velocity and concentration measurements in the wake are in excellent agreement with one another in both the plateau and self-similar wake regions.

3) Turbulent intensity measurements in the plateau show the rms velocity fluctuations to be constant with a value of $u'/[u_\infty - u(o)] \approx 0.25$ as measured by the LDV, indicating the presence of low intensity turbulence.

4) Small-scale boundary-layer turbulence was measured in the wake plateau region.

5) Radial distribution of both velocity and concentration in the plateau region appear to be Gaussian, with the same scale size.

6) Radial velocity distribution measurements in the plateau show maximum turbulent fluctuations to exist at $\eta \simeq 1.0$, the point of maximum velocity gradient.

7) The length of the plateau region was found to increase with increasing flow Reynolds number.

Appendix

The accuracy of the measured probability density function $P(u)$ with scanning Fabry-Perot is determined by the number of velocity samples which occur in the time it takes the Fabry-Perot interferometer to sweep through each velocity bin, the latter time is given by the scan time per free spectral range, T, divided by the finesse, F, of the Fabry-Perot. The number of independent samples per unit time is approximately u_∞/Λ, and the portion of these samples which lie in a given velocity bin is $P(u)/\Delta u$ where Δu is the velocity resolution of the LDV given by $u_{\max}/F$. Noting that $P(\bar{u})2u' \sim 1$ where u' is the velocity standard deviation, it follows that the expected number of independent samples in each velocity bin is given by

$$N_u = \tfrac{1}{2}(T/F^2)(u/u')(u_{\max}/\Lambda)[P(u)/P(\bar{u})] \tag{A1}$$

while the total number of independent samples is

$$N_{\text{Total}} = 2u'u_\infty T/u_{\max}\Lambda \tag{A2}$$

For the LDV configuration used, $T = 0.2$ sec (when set to get only the Doppler shifted signal), $u_{\max} = 1500$ msec and $F \sim 150$. While typical values of u'/u_∞ and Λ were 0.1 and 1–4 mm, respectively. Therefore, $N_u \cong 70[P(u)/P(\bar{u})]$ for $\Lambda = 1$ mm and $17[P(u)/P(\bar{u})]$ for $\Lambda = 4$ mm.

To estimate the standard error in the measured probability density function, we assume entries in a given bin are Poisson distributed so that the variance in the measured number of bin entries, N_i, is given by

$$\langle N_i^2 \rangle > N_u^2 + N_u \tag{A3}$$

and the normalized standard error thus becomes

$$\sigma_N = \left(\frac{\langle N_i^2\rangle - \langle N_i^2\rangle}{\langle N_i^2\rangle}\right)^{1/2} = \left(\frac{1}{N_u}\right)^{1/2} \tag{A4}$$

Since the maximum value of $N_u \approx 70$, the minimum expected error σ_N is 12% while a 45% error can be expected when $P(u)$ drops to 0.1 of its maximum value (i.e., at approximately the $2u'$ point for a Gaussian velocity pdf).

Once the error in $P(u)$ has been established, one can get an estimate of the error in the rms velocity fluctuations, u'.

Let

$$P(u) = \exp\{-\tfrac{1}{2}(u/u')^2\} \tag{A5}$$

Then to a good approximation, the error in the rms velocity fluctuation $\delta u'$, because of the statistical error in $P(u)$, becomes

$$\delta u' \cong \left.\frac{du}{dP(u)}\right|_{u=u'} \sigma_N = e^{1/2}\sigma_N \tag{A6}$$

References

[1] Levensteins, Z. J. and Krumins, M. V., "Aerodynamic Characteristics of Hypersonic Wakes," *AIAA Journal*, Vol. 5, Sept. 1967, pp. 1596–1602.

[2] Schneiderman, A. M., "Measurements of Instantaneous Spatial Distribution of a Passive Scalar in an Axisymmetric Turbulent Wake," *Proceedings of Turbulent Shear Flows*, NATO AGARD CP-93, 1971, pp. 14.1–14.11.

[3] Finson, M. L., "Hypersonic Wake Aerodynamics at High Reynolds Numbers," *AIAA Journal*, Vol. 11, Aug. 1973, pp. 1137–1145.

[4] Townsend, A. A., "The Turbulent Wake," *The Structure of Turbulent Shear Flow*, Cambridge University Press, Cambridge, England, 1956, pp. 131–171.

[5] Demetriades, A., "Mean Flow Measurements in an Axisymmetric Compressible Turbulent Wake," *AIAA Journal*, Vol. 6, March 1968, pp. 432–439.

[6] Avidor, J. M., "Novel Instantaneous Laser Doppler Velocimeter," *Journal of Applied Optics*, Vol. 13, Feb. 1974, pp. 280–285.

[7] Schneiderman, A. M. and Sutton, G. W., "Laser Planogram Measurements of Turbulent Mixing in the Near Wake of a Supersonic Cone," *Physics of Fluids*, Vol. 13, No. 7, July 1970, pp. 1679–1682.

[8] Demetriades, A., "Turbulence Measurements in an Axisymmetric Compressible Wake," *Physics of Fluids*, Vol. 11, No. 9, Sept. 1968.

[9] Patel, V. C., Nakayama, A., and Damian, R., "Measurements in the Thick Axisymmetric Turbulent Boundary Layer Near the Tail of a Body of Revolution," *Journal of Fluid Mechanics*, Vol. 63, Pt. 2, 1974, pp. 345–367.

[10] Cebeci, T., "Eddy-Viscosity Distribution in Thick Axisymmetric Turbulent Boundary Layers," *Journal of Fluids Engineering*, June 1973, pp. 319–325.

[11] Kistler, A. L. and Chen, W. S., "The Fluctuating Pressure Field in a Supersonic Turbulent Boundary Layer," *Journal of Fluid Mechanics*, Vol. 16, 1963, pp. 41–64.

[12] Laderman, A. J. and Demetriades, A., "Mean and Fluctuating Flow Measurements in the Hypersonic Boundary Layer over Cooled Wall," *Journal of Fluid Mechanics*, Vol. 63, 1974, pp. 121–144.

[13] Rose, C. W., "Turbulence Measurements in a Compressible Boundary Layer," *AIAA Journal*, Vol. 12, No. 8, Aug. 1974, pp. 1060–1064.